Exp Astron (2011) 30:165–182
DOI 10.1007/s10686-010-9203-4

ORIGINAL ARTICLE

Generation 2 testbed of Fresnel imager: first results on the sky

Laurent Koechlin · Jean-Pierre Rivet · Paul Deba · Truswin Raksasataya · Thierry Gharsa · René Gili

Received: 15 July 2010 / Accepted: 1 October 2010 / Published online: 12 May 2011

Abstract We present and discuss the first sky images obtained with a second generation "Fresnel Diffractive Array Imager" (FDAI) prototype. These images have been made on high contrast multiple stars (STF-1273 and BU-893), and on Saturn. The focusing objective: a 200 × 200 mm "Fresnel array", is a 50 μm-thick opaque foil featuring approximately 250,000 specially shaped void apertures, corresponding to 696 Fresnel zones. It focusses light by diffraction. This prototype has been installed in parallel to the 76 cm "*grand équatorial*" (17.89 m focal length) at the *Observatoire de la Côte d'Azur*, (Nice, France). The Fresnel array is attached close to the front end and on the side of the 19 m long refractor's tube. The "receiver module" (field optics, chromatic corrector and cameras) is placed at prime focus of the Fresnel array, and attached to the refractor tube close to the rear end. The chromatic correction in the receiver module is adapted to 800 nm, but operates successfully in the two spectral bands used: 630–745 nm and 750–950 nm. This setup has been used to test the on-sky capabilities of the diffractive imaging system in angular resolution, limiting magnitude and contrast, and to experience some of the situations that will be encountered in a future space-borne formation flying configuration. We have obtained high contrast diffraction-limited images of various celestial

L. Koechlin (✉) · P. Deba · T. Raksasataya · T. Gharsa
Laboratoire d'Astrophysique de Toulouse-Tarbes, Université de Toulouse, CNRS, 14 avenue Edouard Belin, 31400 Toulouse, France
e-mail: laurent.koechlin@ast.obs-mip.fr

J.-P. Rivet · R. Gili
Université de Nice Sophia-Antipolis, CNRS, Observatoire de la cote d'Azur, UMR 6202, B.P. 4229, 06304 NICE Cedex 4, France

sources, with a field of view larger than 500″, a resolution of 0.8″ at 800 nm, and a dynamic range better than 10^{-5}.

Keywords Diffractive focusing · Formation flying · High angular resolution · High dynamic range · UV domain · Exoplanets

1 Introduction

The Fresnel Diffractive Array Imager (FDAI) is based on the binary Soret rings plate concept [11]. An orthogonal structure is superimposed to the traditional Soret rings, so that the structure is self-sustained, and is realized by laser carving a thin opaque sheet (no transparent substrate needed). Figure 1 shows a traditional Soret zone plate (left) and a self-sustained Fresnel array (right). This has been described in detail in previous publications [6, 13]. The advantages of this new concept for astronomical imaging is two-fold: first, the incoming light converges without passing through any material or reflecting on any surface. Consequently, no absorption occurs in this part of instrument, and a wide range of wavelengths (practically from 120 nm to 25 μm) would be accessible in a space-borne implementation. Second, the main aperture optical component is a light-weight and thin opaque foil with void apertures, much lighter than an equivalent diameter telescope.

The released tolerances compared to classical optics polishing and positioning allow high quality wavefronts even at very short wavelengths. Moreover, the small weight of a Fresnel array, compared to standard optics with similar

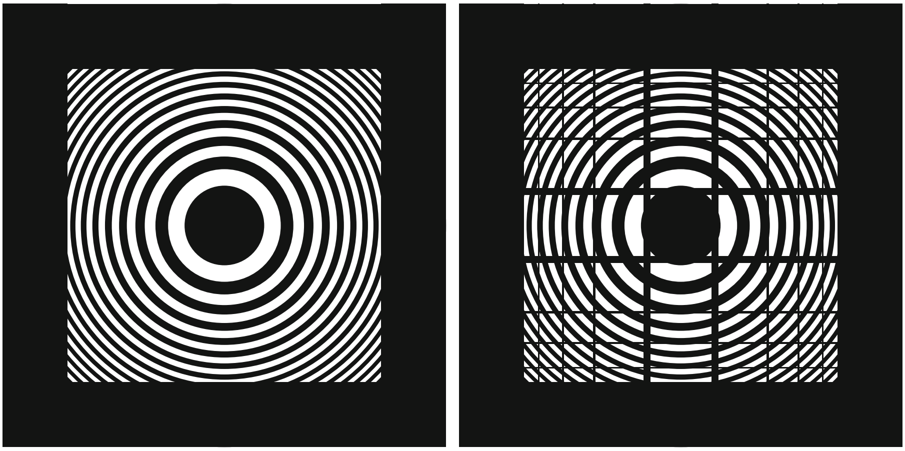

Fig. 1 *Left*: Circular (Soret) zone plate. *Right*: an example of self-sustained Fresnel array, with 15 Fresnel zones (on the half diagonal). The bars holding the rings are in phase relation with them: one every n^{th} ring. In the Fresnel array of the Generation 2 prototype, there are 696-Fresnel zones and 2×232 bars. This corresponds to $\simeq$250,000 arc-shaped holes. Some kind of apodization has also been introduced: the rings' thickness ratios vary from center to edge

collecting power, makes this concept particularly well suited to large space-borne telescopes: from 4 to 40 m diameter or more, with focal lengths from 400 m to 40 km that would be accessible with a two-spacecraft formation flying.

Before sending to space an instrument involving a new optical concept, it has to be qualified with ground based testbeds. In the recent years, we have built several generations of such equipment. The first two were laboratory experiments to validate the high dynamic range and diffraction-limited imaging capabilities on artificial sources [8, 14]. In addition, an end-to-end dedicated numerical simulation tool has also been developed [14], the results of which have been successfully compared with experimental data.

The “Generation 2” testbed under consideration in this article is dedicated to on-sky operation. It is the result of a step by step evolution. The migration stages from generation 1 to generation 2, and the work done from 2008 to November 2009 are presented in Rivet et al. [15]. The present paper discusses the final implementation and the on-sky results obtained with the fully featured generation 2 prototype, on “well known” but difficult sky objects such as high contrast, faint, and close binary stars, or planets.

Sections 2 and 3 describe why and how we have implemented this testbed. The optical and mechanical design, and the reduction procedure are presented in Section 4. The results obtained on several sky sources (binary stars, planets and satellites, deep sky objects) are discussed in Section 5, and the outline of a future space mission is depicted in Section 6.

2 Why a Generation 2 testbed?

Although we propose this new concept for space applications with very large apertures and very long focal lengths, its validation has to be made with a limited budget, hence with a small diameter aperture and a focal length adapted to a ground-based setup. Nonetheless, the validation has to be as precise and realistic as possible.

The first laboratory testbed (Generation 1) has been successful in demonstrating the high contrast imaging capabilities of Fresnel imagers on artificial sources: 10^{-6} [9]. This has motivated the decision to proceed further and to tackle with the broad diversity of spectral distribution, contrasts, angular sizes and brightness offered by astronomical sources in real conditions. Indeed, it was important to assess the efficiency of this new concept in observing conditions, closer to those of a real space instrument. The goal was to prove that, even in real observing conditions, Fresnel imagers can produce astronomical images with contrast and resolution equivalent or better than provided by regular telescopes of equal aperture.

As current technology limits the size of the smallest aperture to 20 μm, the focal length of a 200 × 200 mm cannot be smaller than 18 m for observations around 800 nm. Thus, we have chosen to use the tube of a large astronomical refractor as a giant optical bench. That is why the historical 76 cm refractor (focal length 17.89 m, tube length 19 m) of the *Observatoire de la Côte d'Azur* (Nice, France), has been chosen to hold our Generation 2 prototype.

The two modules of Generation 1 testbed were modified to fit safely on the refractor's tube, leading to the so-called "Generation 1.5" prototype [15]. The first steps of implementation started in June 2009, and the system was operational with nominal performances in October 2009.

The tests carried on with this generation 2 testbed addressed the following issues:

– angular resolution
– field width and spectral bandpass
– dynamic range
– limiting magnitude

These tests aim also to study practical problems of importance for future space-borne applications, such as the accuracy required on the relative position and attitude (orientation) of the receiver module and of the Fresnel array module, in order to have an efficient chromatic correction using a scheme adapted from Schupmann [10] and Faklis and Morris [2]. The issue of turbulent tip-tilt and its real-time correction has also been addressed.

3 Setting up the Generation 2 testbed

The second generation testbed had to demonstrate the on-sky efficiency of the FDAI concept in real (ground-based) observing conditions. Indeed, experimental feedback was needed on how such optical combination withstands non-ideal conditions (thermal fluctuations, mechanical flexions, vibrations, misalignments, atmospheric turbulence, poor celestial guiding). For cost—and time—efficiency, we have chosen to install the FDAI in parallel to an existing astronomical instrument, which was expected to act both as a mechanical mounting and as a reference for optical performances comparisons.

3.1 Implementation constraints

Since the 76 cm diameter refractor which was available for this experiment is part of a protected historical monument, some constraints had to be taken into account when designing the mechanical interfaces between the FDAI and the tube of the refractor. Indeed, the two elements (the Fresnel array module and the receiver module) had to be assembled on the tube without any irreversible operation.

Using an existing instrument as a mechanical support yields another limitation: the modules must not be too heavy. Otherwise, excessive mechanical flexions of the refractor's tube may result, and the motor drives may have insufficient torque to move the instrument correctly. The total weight of each module had to fall well below 40 kg.

Another design constraint comes from the flexions of the tube and their consequences on the chromatic correction, which requires a good alignment of the receiver module with the Fresnel array module. Since both modules are at opposite ends of athe 19 m long metallic tube, a flexion of the tube results in a misalignment, and poor chromatic correction. Thus, the orientation of the receiver module with respect to the Fresnel Array needs to be fine-tuned. Moreover, the mechanical flexion of the refractor's tube varies when the instrument's orientation changes. As a consequence, the relative orientation must be corrected frequently.

All these issues have crucial influence on both the "external design" of the instrument (the way the two modules are connected to the existing refractor) and on the "internal design" (the way the optical components are arranged within each module). Both issues are discussed hereafter.

3.2 "External" design

Figure 2 shows the overall geometry of the setup, including the refractor's tube, the Fresnel array module, and the receiver module. Both modules of the Fresnel imager are connected to the refractor's tube by massive mechanical stands, which are fastened to the tube by a pair of stainless steel belts. Those belts are stiffened by stay tensioners (see Fig. 3). This mechanical solution, although fully reversible and harmless for the refractor's tube, revealed to be steady enough for our purpose: the image drifts due to residual flexions are small enough to be well corrected by a tip-tilt corrector and/or a "shift-and-add" postprocessing.

The Fresnel array module stand is rather simple, since no runtime fine-tuning is required usually. Casually, it may happen that the diffraction spikes of the array exactly coincide with an astronomically relevant feature in the final image. In this case, the array has to be rotated around its optical axis. The

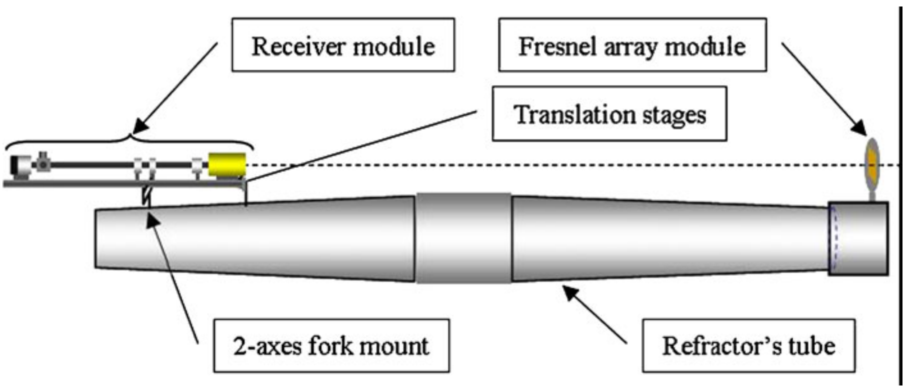

Fig. 2 The global structure of the instrument (not to scale). The refractor's tube is 19 m long, and the optical rail is 2 m long. The optical axes of the refractor and of the Fresnel imager are parallel

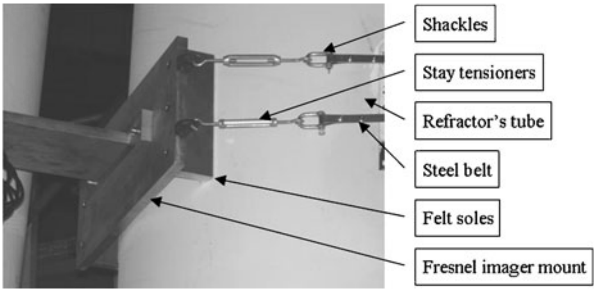

Fig. 3 Non-destructive mounting system. The mount is fastened to the refractor's tube by two stainless steel belts, the tension of which is adjusted with four stay tensioners. The felt soles prevent damage of the refractor's coating

mount has been designed consequently. This is the only degree of freedom that may be modified in runtime on the array module. Figure 4 displays this module.

The receiver module is much more complex and requires an elaborate mount. Basically, this module is a 2 m long optical rail with an "X"-shaped cross section. Since it has to be oriented accurately towards the center of the Fresnel array, it cannot be rigidly connected to the refractor's tube. A good chromatic correction requires frequent correction of this module's orientation. Thus, the rail is connected to the tube by a two-axis fork mount (see Fig. 5). The intersection of those axes is supposed to be very close to the center of gravity of the receiver module, so that the module is close to a neutral equilibrium, and very few strength is needed to modify its orientation. This fork mount bears the weight of the receiver module. It is thus firmly bolted

Fig. 4 *Left*: the Fresnel array module on its mechanical stand. *Right*: the same module, mounted on the refractor's tube. The orientation of the square aperture (hence of its PSF spikes) can be adjusted by rotating the cell holding it. The cell has been rotated by 45° between the two figures

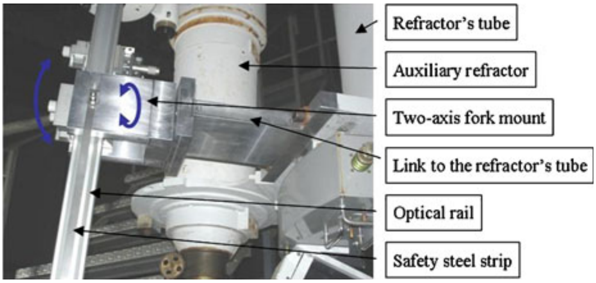

Fig. 5 The two-axes fork mount connecting the receiver module to the refractor's tube. The foot of the fork mount is tightly bolted on an existing structure of the refractor (the sole of a former auxiliary finder)

onto the refractor's tube through the already existing mechanical interface of an auxiliary finder.

To drive smoothly and accurately the global tip-tilt motion of this module, a third stand is connected to the tube, with the same kind of steel belts as for the Fresnel array module. This stand is connected to the tip of the receiver module's optical rail through a pair of crossed electrically-operated translator stages (see Fig. 6). Thus, the orientation of the rail can be remote-controlled easily and accurately during runtime.

3.3 "Internal" design

In Fresnel imagers, the incoming light encounters first the Fresnel array, a 200×200 mm thin metallic foil with laser-carved apertures (696 apertures along a semi-diagonal). The second component on the optical path is a field optics located close to the focal plane of the Fresnel array (first diffractive order), 18 m downstream (see Fig. 7). This field optics is a 150 mm Maksutov telescope with 1,800 mm nominal focal length. The field is limited by an off-axis 45 mm circular field stop, fitted between the central obscuration and the edge of the Maksutov aperture, and placed in front of the Maksutov meniscus. The

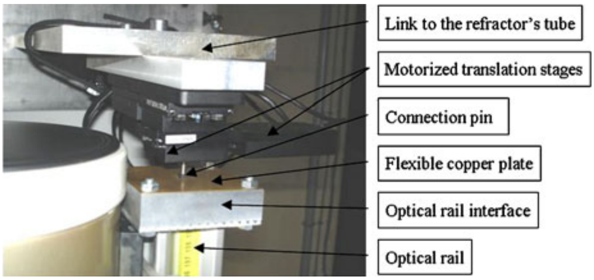

Fig. 6 The crossed XY translator stages connecting the optical rail of the receiver module to the refractor's tube. Since the optical rail is on a fork mount, the XY translation stages acting on its upper end, modify the orientation of the whole receiver module with respect to the Fresnel array module. The fine tuning of the chromatic correction is obtained by electrically controlling these translation stages

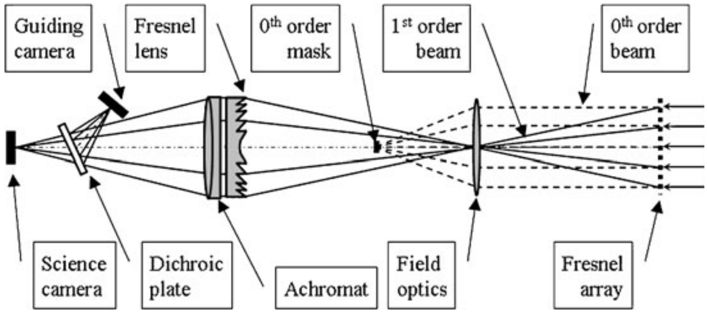

Fig. 7 The optical scheme of the Generation 2 Fresnel imager (not to scale). The light beam from the zero order of diffraction is represented by *dashed lines*, whereas *solid lines* are used for the first order beam

field optics makes an image of the entrance pupil (the Fresnel Array) onto the chromatic corrector, a 58 mm fused silica blazed Fresnel lens with 702 zones. At nominal setting, each Fresnel zone of the main array is imaged upon the corresponding zone of the chromatic corrector.

The 6 additional zones of the chromatic corrector (702 compared to 696) make possible a relative shift of the pupil versus blazed lens, without vignetting, in case a linear dispersion of specified amplitude and orientation is requested in the image plane. The linear dispersion (or no dispersion) is set by the translations stages atop the optical rail.

Then, a custom-made doublet (diameter 64 mm, optimized for 800 nm with focal length 350 mm) produces a final image in the cameras module. This baffled module contains two identical *Andor Luca R* EMCCD cameras, one for science and one for guiding, plus a beam splitter between the science and the guiding channels: a square 50.8×50.8 mm dichroic plate with a sharp cutoff at 740 nm. The quantum efficiency of theses cameras peeks at 65% for 600 nm, and remains above 40% between 400 nm and 820 nm, and 25% at 900 nm.

Like a diffraction grating, the Fresnel array transmits light at several orders. Only the light from order $+1$ is desired at the detector focus. A proper design of the Fresnel array almost suppresses the light from orders ± 2 and all non-zero even orders. The light from order -1 is unfocussed and contributes to the background at a very low relative level of about $(1/4k_{\max})^2$, where $k_{\max}$ is the number of Fresnel zones from center to edge.[1] This amounts to 1.3 10^{-7} for $k_{\max} = 348$, The light from orders ± 3 and above are so dim and unfocused that they can also be neglected. However, the light from order 0, which is not focused and spread over the image plane, has to be rejected, since it would hamper the high dynamics capabilities for the instrument. For this sake, an opaque mask stands exactly where the order 0 light focuses, that is, in the image

[1]The number of Fresnel zones from center to edge is half the number of zones from center to corner, in the case of a square aperture.

focal plane of the field optics. This mask is a 2 mm diameter disk, suspended to a pair of crossed 30 μm synthetic wires stretched across two diameters of a metallic barrel. In this plane, the light beam from first order has a diameter of 30 mm. Thus, the order 0 rejection mask does not block a significant amount of the scientifically relevant light. The zero order blocking setup would be slightly different for the real size space borne system. During the alignment phase, this zero order mask must be visible on the final image. Thus, it can be illuminated by a series of blue LEDs (400 nm wavelength), so as to be visible on the guiding camera (the one which receives the short wavelengths from the dichroic plate). This choice of a short wavelength to illuminate the zero order rejection mask deserves an explanation: the light focused by the Fresnel array at order 1 is chromatically corrected by the order -1 of the Fresnel lens. Thus, the blaze angle of this lens has been optimized to minimize the amount of light wasted in all diffraction orders but the order -1, at least in the nominal spectral band of the instrument (750 to 850 nm). Thus, in this spectral band, very few light is transmitted by the Fresnel lens at order 0. Consequently, the light from the zero order rejection mask, focused onto the camera's sensor by the order 0 of the Fresnel lens, would be too faint to be detectable. However, this doesn't hold for a wavelength such as 400 nm, well outside of the nominal spectral band for which the Fresnel lens has been blazed. So, this bue light reaches the camera as expected, making the zero order rejection mask clearly visible during the preliminary alignment phase.

The initial choice of the bandpass was between 750 and 850 nm in order to minimize the atmospheric diffusion and absorption by H_2O. In addition, the seeing is also better in this band. The atmospheric O_2 absorption line at 760 nm blocks only a small part of the light, as it is relatively narrow. Some of the results presented in this article have been made in a second spectral band, between 650 and 750 nm, for some hot objects such as Sirius-B. Finally a third set of data on nebulae (M42) has been acquired with a 12 nm bandwidth H_α filter.

For various reasons (flexions, polar misalignments, turbulence), the position of stellar images is not steady on the sensor. To compensate as much as possible for these unwanted motions, the final achromat is mounted on an XY piezzo-actuator. This actuator is driven according to the indications of the guiding camera, by a computer running a real-time PID control loop program with a fast centroid detection algorithm. The servo loop running at 100 Hz is able to compensate for mechanical drifts (flexions, sidereal guiding defects), and even for slow atmospheric tip-tilt. However, in order to smear out some inhomogeneities in the target background of the cameras, we chose to disconnect the tip-tilt corrector for part of the observation campaign. It was replaced by a software shift-and-add postprocessing algorithm.

The EMCCD cameras were chosen for their sensitivity, and their cost efficiency, but they appeared to be less than optimal for high dynamics. The choice of a more expensive backlit CCD would have greatly improved the quality of data. Indeed, the ghosts due to the diffraction patterns on the sensor and the irregularity of the target background would have been avoided. In addition, the global efficiency of the instrument would be enhanced by a anti-reflect coating on the entrance window of the camera.

All the aforementioned optical elements, except the entrance Fresnel diffractive mask belong to what we named “the receiver module” in Section 3.1.

3.4 Alignment procedure

The proper alignment of this Fresnel array system is a critical issue for high dynamics. There are two main elements that need special care: the blazed Fresnel lens which has to be superimposed to the image of the main Fresnel array through the field optics, and the zero order mask, which has to be properly centered.

For the blazed Fresnel lens, the initial alignment procedure involves the daytime sky background to lighten the Fresnel array. Then, a lens and an eye-piece are inserted on the optical path close to final focus, to show a pupil plane downstream. Thus, both the Fresnel zones of the main array and the Fresnel zones of the blazed lens are visible in the eyepiece. The correct orientation for chromatic correction is reached when, by setting the attitude of the receiver module, the Fresnel zones of the blazed lens are seen superimposed to those of the main array. During nighttime observations, due to flexions of the refractor tube, the orientation of the receiver module needs to be fine-tuned every few minutes. As the main Fresnel array cannot be illuminated during data acquisition, the correction is based on residual dispersion (for compact objects) or “moiré” fringes in the pupil plane (for extended sources). For a future space mission, the pupil alignment will be maintained by a proper attitude control of the receiver spacecraft. The precision required is comparable to the angular resolution of the field optics: a 4.5 cm aperture in our testbed, (60 cm for a space version with a 4 m membrane array).

For the zero order rejection mask, a proper alignment has to be done each night, on a stellar image. The image has to be well centered in the field. Then the zero order mask illumination LED is switched on. The mask becomes clearly visible on the guiding camera, superimposed to the stellar image. It is then easy to translate the rejection mask to center it on the stellar image, before starting the high dynamic range data acquisition.

3.5 Some issues about high dynamics

Our optical setup does not contain a coronagraphic mask. Thus, the performances in terms of dynamic range rely only on the quality of the Fresnel array’s PSF, on the rejection of stray light, and on the quality of the detector. The results of the first observation has shown to which extend the sake of high dynamics is demanding in terms of the detector’s quality. The structure of the detector itself produced two kinds of artifacts: diffraction effects, and electronic crosstalk. The pixels of the *Andor Luca R* EMCCD sensor reflect and diffract a small part of the incident light. A fraction of this reflected/diffracted light is reflected back to the sensor by its uncoated window. Thus, bright PSFs produced spurious cross-shaped diffraction spikes, in addition to the expected spikes of the Fresnel array. Moreover, at high dynamic range, some electronic "crosstalk" between distant bright and faint pixels is responsible for background irregularities unnoticed in normal conditions. These artifacts produce unwanted non random features in the image, which cannot be averaged out nor flat-fielded, since they are linked to bright PSFs. These effets were underestimated during the prototype design phase, and as we could not afford a very high grade camera, we found workaround solutions to get rid of them, at least partially. To do so, we let the target drift slightly in the field of view, to smear out the static artifacts by the shift-and-add processing.

In order to implement the tip-tilt correction, we needed to split the light into a guiding channel and a science channel. For this, we use a dichroic plate. Our results also showed that optical filters or dichroic beam splitters usually considered of "high quality" can generate ghosts by multiple reflections. This effect, which is considered as minor for standard applications, becomes relevant when high dynamics is concerned.

To improve the dynamics, the spectral bandpass needs to be limited by filters for two reasons. First, our chromatic correction scheme is effective at all wavelengths for the light transmitted through the diffraction order -1 of this Fresnel lens. Only this light is chromatically corrected and focused on the detector. Far from its blaze nominal wavelength (800 nm), the lens transmits a small fraction of the incoming light through other orders. This uncorrected and unfocussed light is shed all over the image plane and causes a nearly uniform haze. This small fraction of the light (from 0 to 2%) is diluted over a wide area and does not significantly limit high dynamic range if the working bandpass is limited to ± 150 nm around the nominal wavelength (800 nm). Second, the longitudinal chromatism of the main Fresnel array also yield a limitation of the accessible bandpass: for wavelengths far from nominal, the first order focus of the Fresnel array is far upstream or downstream from its nominal position. This does not affect the dynamics, provided the beam is not vignetted by the field stop (a 45 mm circular hole located in front of the Maksutov telescope used as a field optics; (see Fig. 8 and Section 3.3).

If vignetting occurs, a relatively bright and lower-resolution PSF is superimposed to the nominal high-resolution one. A loss in both resolution and dynamics would result. This feature requires to limit the working bandwidth to $\Delta\lambda = \sqrt{2}\lambda D/C$, where D is the diameter of the field stop at primary focus, and C the size of the square aperture. For example, a 200 mm Fresnel array and a 45 mm field stop, leads to a bandwidth limitation of $\Delta\lambda/\lambda = 30\%$, which corresponds to ± 120 nm around the nominal wavelength (800 nm). As we accepted some vignetting concerning the corners of the main square aperture at off-center wavelengths, the tolerance was increased to ± 150 nm.

To limit the bandpass properly, we have added on the optical path a long-pass filter, which eliminates wavelengths shorter than 630 nm. Wavelengths longer than 920 nm are naturally eliminated, both by atmospheric H_2O

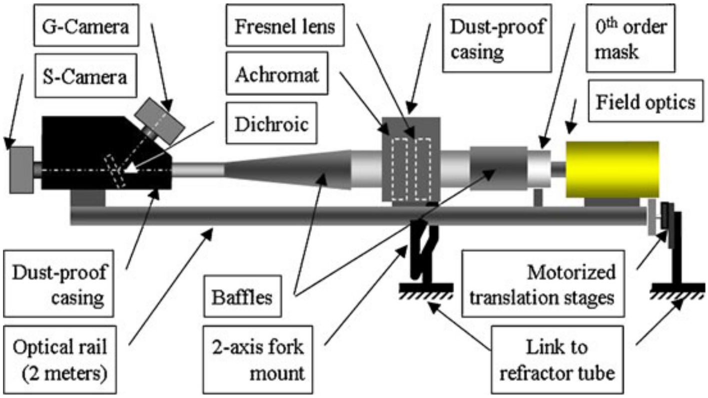

Fig. 8 The setup of the Generation 2 Fresnel imager (not to scale). The 45 mm field stop (not represented) is located immediately upstream of the field optics (a Maksutov telescope)

absorption, and by the waning sensitivity of the detector (less than 6% global throughput above 920 nm).

4 Data acquisition and processing

The main goal of this first set of on-sky experiments was to assess the high dynamics capabilities of the Fresnel imager. In this context, flat-field correction would have been of little interest. Moreover, they would have introduced some unwanted noise. Consequently, the raw images were only corrected for the sky background brightness.

As explained in Section 3.3, some data sets were obtained without any real-time active tip-tilt correction. For those data, we apply a shift-and-add algorithm with frame selection (lucky imaging). Let's now describe in some detail the data acquisition procedure and processing.

4.1 Data acquisition procedure

The acquisition software delivers data cubes with up to 1,000 individual frames, and stores them according to the FITS image standard. For each sky target, several sequences of 10 data cubes were taken. The chromatic correction needed to be checked and sometimes fine tuned, at least every 15 min, due to the combined effect of mechanical flexions and atmospheric dispersion (see Section 3.3).

Since the sky background is high and rapidly varying, series of sky background images acquisitions were performed after each set of 10 science sequences, with the same exposure time and the same filters.

Even when the tip-tilt corrector was off, the rapidly refreshed images of the guiding camera were displayed by the guiding computer. This was useful to check for unwanted drifts of the image. Thus, if needed, the image was manually centered on during the readout phase which follows each data cube acquisition inside a sequence.

4.2 Data processing

The first step of the data processing pipeline is to process the sky background sequences of data cubes. From each data cube in a sky background sequence, one extracts a unique sky background image by a clipped averaging procedure: for each pixel of the final image, the level values of the corresponding pixel from all the individual frames in the cube are collected and sorted. The 1% smallest and the 5% highest are considered as non significant and thus rejected. The remaining values are averaged. This procedure is performed with all the cubes in the sequence, leading to one sky background image per data cube. Then a "global sky image" is obtained by a simple averaging of the resulting individual background images.

Then, one processes the sequence of science data cubes corresponding to the sequence of sky background data just processed. For each science data cube in the sequence, the following operations are performed:

1. Subtract the master sky background image from each individual frame of the cube.
2. On a chosen reference image (not necessarily from the same data cube), determine the centroid of the brightest object. This position will be chosen as "reference point".
3. For all other frames, compute the centroid in a 50×50 to 200×200 pixels window around the reference point, and shift the frame so that the centroid coincides with the reference point. The centroids and shifts are at a 0.2 pixels or better precision.
4. Perform a clipped averaging of all recentered individual frames.

This leads to one compound image per data cube. Then, all are summed to form the science image of each sequence.

5 Results in resolution and high dynamic range

Our sky targets have been chosen to challenge different aspects of the Fresnel imager. We aim at sampling the "dynamic range versus angular separation" space: from the data obtained on binary stars, we measure a dynamic range for a given angular separation, then compare it to what can be expected from a numerical instrument model. We checked how close to this model we could be with sky observations (see Fig. 9).

We remind that this instrument model is extendable to large Fresnel arrays, and shows that for 4 m arrays, dynamic ranges of 10^{-7} to 10^{-8} can be reached on raw images. For small, 200×200 mm arrays, the predicted dynamic range is around 10^{-6}.

Fig. 9 Binary stars observed with Generation 1.5 prototype (*red diamonds*) and Generation 2.0 (*green squares*). Some V and R magnitudes of the faint component star are mentioned. The curve defining the blue shaded zone below corresponds to the limiting dynamic range (in stellar magnitudes) as a function of angular separation (in arc seconds) as sampled from the numerically computed PSF of our Fresnel imager prototype

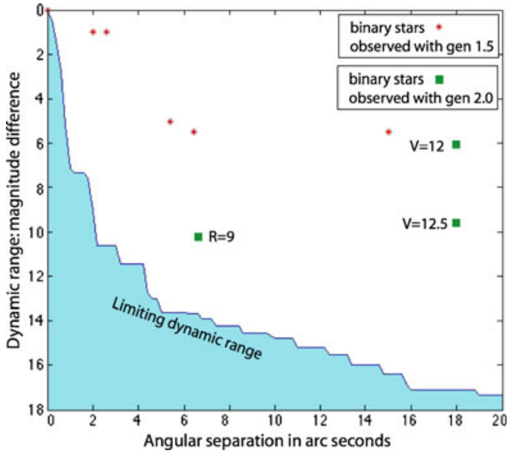

5.1 Multiple stars

The results with the 200 × 200 mm aperture Fresnel imager and an *Andor Luca R* EMCCD concern two multiple star systems: BU 893 ABC (alternative identifiers: SAO 58716, HD 41162) and STF 1273 AD (alternative identifiers: SAO 117112, HD 74874). BU 893 ABC has separations $AB = 18.1$" and $AC = 85.4$", spectral types K0 and A2 for components A and B, and V magnitudes 6.34, 12.7 and 11.6. STF 1273 has a separation of 18.1″, spectral type $F8$ for component A, and V magnitudes 3.49 and 12.5. Figures 10 and 11 show these two multiple star systems with high magnitudes differences. A magnitude

Fig. 10 Binary star BU 893 AB (HR2137), with a 6 magnitudes difference between the central star and its companion. Image taken on January 22nd, 2010, with 300 s exposure time, without intensification, in the bandpass 745–900 nm. V magnitudes 6 and 12, separation 18″. The companion is well detected, although a diffraction spike of the brighter star's PSF happens to be almost exactly superposed. Several other stars are visible in the field

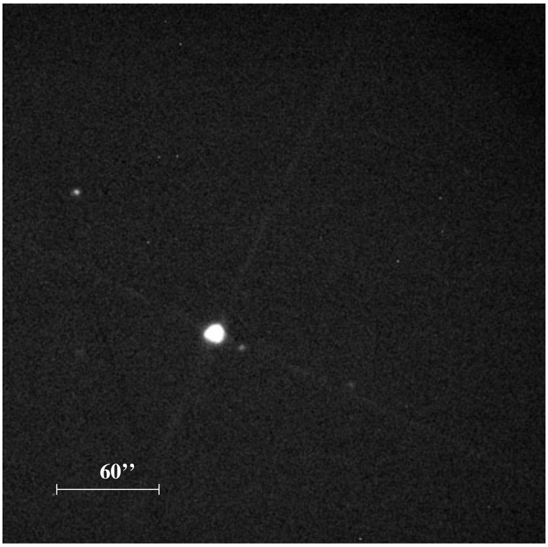

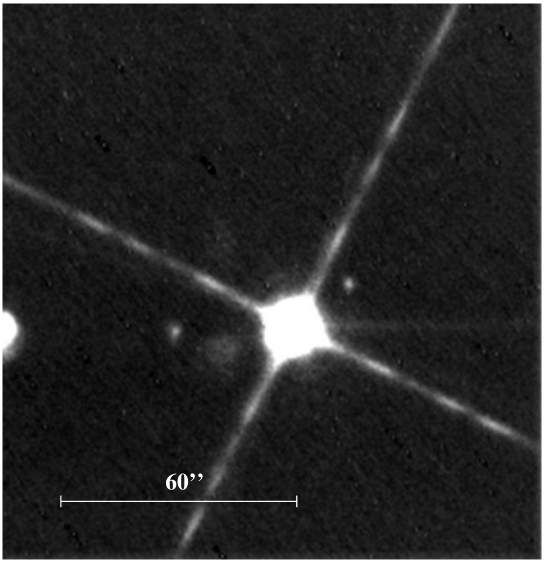

Fig. 11 Multiple system STF 1273, with a 9 magnitudes difference between the central star and the companion on the upper right. High contrast image taken on March 14th, 2010, exposure time 20 s with EM intensification, bandpass 630–743 nm. In this image, only one companion of STF 1273-A (magnitude 3.5) is shown: STF 1273-D: of magnitude 12.5, at 18″ separation. The other companions are either unresolved or out of the field. The spot on the left and blobs at the left side of the image are artifacts: multiple reflections of the central star in the dichroic plate used for splitting the beam between "science" and "guiding" channels

difference of 9 as in STF 1273 AD, corresponds to a brightness ratio of 4,000 to 1. The other components of the multiple system STF 1273 are either not resolved, or out of the field.

5.2 Saturn

The planetary disk of Saturn covers 19″, and 45″ with its rings. It has been imaged with four of its satellites in the field: Titan, Rhea, Dione, Enceladus, which are evidenced in the same acquisition when adjusting the contrast and luminosity (see Fig. 12). Several artifacts are present: the four diffraction spikes convolved with the planetary disk, an unfocussed reflection originating from the dichroic beam-splitter, smearing from the CCD camera, and reflection from the sensor window.

6 Space mission proposed

We have developed the Fresnel array initially for direct imaging and spectral analysis of exoplanets [6]. There are many other ways to reach that goal: nulling interferometry [5, 7], coronagraphy [12], occulting masks [1].

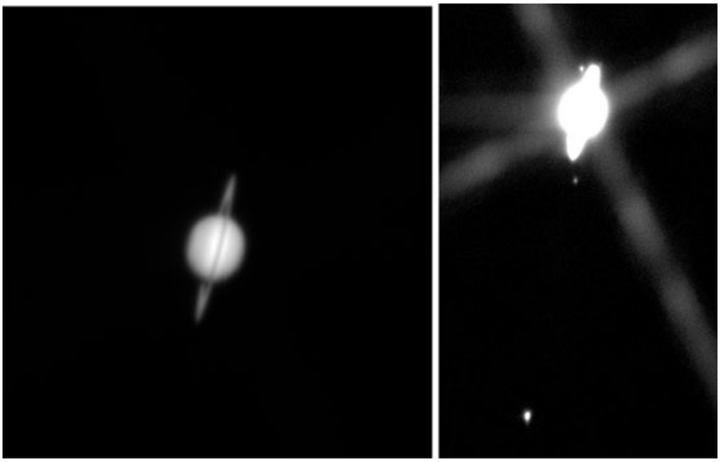

Fig. 12 Disc of Saturn and rings. 200 exposures of 0.2 s each averaged, taken on February 13th, 2010 at 01 : 15 UT with the 200 × 200 mm aperture diffractive Fresnel imager, equipped with an *Andor Luca R* EMCCD camera. Satellites of Saturn are visible on the same data set, using a square root brightness scale: Titan at the bottom, Dione below the rings, Rhea on the upper left, and Enceladus appearing on the upper right, close to the rings. Spectral bandpass 650–663 nm

Now we come up with our diffractive imaging concept, which has a much broader scope than the field of exoplanets, but this is not to our advantage: at present, the rationale of space agencies is to start from a problem to be solved, then launch into space a spacecraft designed with the best suited solution for this problem, and not the other way around: to start from a solution: launch a new technology instrument, then expect observing run proposals to explore the related problems (science cases) that it could solve! As far as we know, this second situation has occurred only for a few very large projects such as LISA or PLANCK, involving worldwide cooperation, and thoroughly tested, space qualified optical concepts.

Although, to our point of view, both approaches are complementary, the second is more risky, but has better chances to bring unexpected and important discoveries. Space agencies don't take risks, and we understand it, so we plan to propose a well defined mission for this yet unqualified concept in space: the future Fresnel array mission will be centered on UV science cases. The UV domain is rich in puzzling objects such as very young planetary systems, and the interstellar medium in which they form [4]. It is also suitable for the study of exoplanets atmospheres, as proposed by Lecavelier des Etangs and Ehrenreich [3].

Furthermore, the UV domain has been very little explored at high angular resolution, as the large existing space telescopes were not diffraction-limited. This is no longer the case if a large (e.g. 4 m) Fresnel imager, is launched in space: its high wavefront quality would provide unprecedented angular resolution and dynamic range in the UV. A 4 m aperture Fresnel imager in orbit around L2, with a 7 mas resolution and 10^{-6} dynamic range, should remain within the cost limits of an "M-class" ESA mission that could be launched in the 2025s.

A generation 3 prototype for concept validation in the UV is under construction, and the optical scenarios for space are reviewed in Deba et al. [16].

Fresnel imagers have two hurdles to overcome before they can be considered seriously by space agencies: show the formation flying requirements they imply are less stringent than in other projects, and show the 7% throughput of the main aperture can be compensated by an increased size at equal price. This can be done with intermediate steps.

The first of these two items could be dealt with, by a micro-satellite mission of a few days or weeks in low orbit, having the optical aperture and intermodule distance comparable to our generation 2 testbed, but free flying and involving the most basic formation flying system.

The second item: developing large membrane diffractive arrays at reasonable cost, is presently under study by ESA contractors in ground-based facilities.

7 Conclusion

We have proven now that, despite a global throughput of the main array (only 6% of the incoming light reaches the primary focus), Fresnel imagers behave honorably compared to reflective or refractive optics of the same size. For example, we have been successful in imaging high contrast multiple star systems (magnitude difference: 9 in V band, 8.55 in I band). We have also imaged the two satellites of Mars with a 200×200 mm aperture Fresnel imager. To the best of our knowledge, this has only been done before with telescopes 300 mm or larger in diameter. Moreover, the images we obtained during nights with low atmospheric turbulence are near diffraction-limited (see our image of Saturn in Fig. 12).

Future developments regard both ground-based and space-borne projects. The UV domain is one possible niche for a first space mission using this young concept.

Most important to us is cooperation, specially with people concerned by the potential science cases in astrophysics that this new concept opens: solar system objects, stellar physics, reflection nebulae, accretion disks and planetary systems formation, exoplanet study and detection of life, Active Galactic Nuclei, and the many other fields of science that may be opened.

Acknowledgements This work has been funded by CNES, Université de Toulouse, CNRS, Fondation STAE, and made possible thanks to the involvement of many people at Observatoire Midi Pyrénées and Observatoire de la Côte d'Azur. We are specially thankful to Jacqueline Platzer, Driss Kouach, Bruno Dubois, Marcel Belot, Marin Cortial, Jean-Jacques Bois, Carine Marchive, Thierry Mallet, and the "Service de Mécanique Mutualisé" at the Observatoire de la Côte d'Azur.

References

1. Cash, W.: Detection of Earth-like planets around nearby stars using a petal-shaped occulter. Nature **442**, 51–53 (2006)
2. Faklis, D., Morris, G.M.: Broadband imaging with holographic lenses. Opt. Eng. **28**(6), 592–598 (1989)
3. Lecavelier des Etangs, A., Ehrenreich, D.: A large UV-optical telescope for characterization of the atmospheres of extrasolar planets and satellites. In: Favata, F., Sanz-Forcada, J., Gimènez, Ì., Battrick, B. (eds.) 39th ESLAB Symposium on Trends in Space Science and Cosmic Vision 2020, 19–21 April 2005, Noordwijk, The Netherlands. ESA SP-588. European Space Agency, 73L (2005)
4. Gomez de Castro, A.-I., Lecavelier, A., D'Avillez, M., Linsky, J.L., Cernicharo, J.: UV capabilities to probe the formation of planetary systems: from the ISM to planets. APSS **303**, 33–52 (2006)
5. Ollivier, M., Mariotti, J.-M., Léger, A., Skulic, P., Brunaud, J., Miche, G.: Nulling interferometry for the DARWIN space mission. C. R. Acad. Sci., Sér. IV Phys. **2**(1), 149–156 (2001)
6. Koechlin, L., Serre, D., Duchon, P.: High resolution imaging with Fresnel interferometric arrays: suitability for exoplanet detection. Astron. Astrophys. **443**, 709–720 (2005)
7. Martin, S.R., Gappinger, R.O., Loya, F.M., Mennesson, B.P., Crawford, S.L., Serabyn, E.: A midinfrared nuller for Terrestrial Planet Finder: design, progress, and results. In: Coulter, D.R. (ed.) Techniques and Instrumentation for Detection of Exoplanets. SPIE Proc., vol. 5170, pp. 144–154 (2003)
8. Serre, D., Koechlin, L., Deba, P.: Fresnel Interferometric Arrays for space-based imaging: testbed results. In: SPIE Proc., vol. 6687-OI (2007)
9. Serre, D.: L'imageur interférométrique de Fresnel: un instrument pour l'observation à haute résolution angulaire. Ph.D. thesis, Université Toulouse III (2007)
10. Schupmann, L.: Die medial-fernrohre: eine neue konstruktion für grosse astronomische instrumente. Teubner B G (1899)
11. Soret, J.-L.: Sur les phénomènes de diffraction produits par les réseaux circulaires. Arch. Sci. Phys. Nat. **52**, 320–337 (1875)
12. Trauger, J.T., Traub, W.A.: A laboratory demonstration of the capability to image an earth-like extrasolar planet. Nature **446**, 771 (2007)
13. Koechlin, L., Serre, D., Deba, P., Pellò, R., Peillon, C., Duchon, P., Gomez de Castro, A.I., Karovska, M., Désert, J.M., Ehrenreich, D., Hebrard, G., Lecavelier des Etangs, A., Ferlet, R., Sing, D., Vidal-Madjar, A.: The Fresnel interferometric imager. Exp. Astron. **23**, 379–402 (2009)
14. Serre, D.: The Fresnel imager: instrument numerical model. Exp. Astron. (2011). doi:10.1007/s10686-010-9200-7
15. Rivet, J.-P., Koechlin, L., Raksasataya, T., Deba, P., Gili, R.: Fresnel imager tetbeds: setting up, evolution, and first images. Exp. Astron. (2011). doi:10.1007/s10686-011-9213-x
16. Deba, P., Etcheto, P., Duchon, P.: Preparing the way to space borne Fresnel imagers. Space scenarios optical layouts. Exp. Astron. (2011). doi:10.1007/s10686-010-9202-5